WEP Warwick Evans Publishing

International Journal of Natural Resources and Environmental Studies

ISSN: 3006-2012 (Print), ISSN: 3006-0834 (Online) | Volume 3, Number 3, Year 2024
DOI: https://doi.org/10.62051/ijnres.v3n3.11
Journal homepage: https://wepub.org/index.php/IJNRES/index

Modeling of Cutting Mechanics Analysis of Diamond Core Bits

Jianlin Yao, Bin Liu, Kuipeng Yao

CCDC Drilling & Production Technology Research Institute, Guanghan 618300, China.

ABSTRACT

Diamond core bits are essential tools for coring operations in deep formations during oil and gas drilling projects. By establishing a cutting mechanics calculation model for diamond core bits, this study investigates the changes in bit load and torque under the influence of key factors such as bit cutting structure, rock strength, and diamond distribution density. This research is significant for optimizing bit structure, enhancing coring drilling efficiency, and prolonging bit lifespan. This paper conducts modeling analysis of the cutting element loads for various shaped diamond particles, including rectangular, triangular, cylindrical, and spherical shapes. Based on this, a cutting mechanics calculation model for axial and tangential forces of granular spherical diamonds is established using the fundamental principles of elastoplastic mechanics. Consequently, a set of methods for calculating and analyzing the working loads of diamond core bits is developed. The findings of this paper provide a theoretical basis for studying the rock-breaking mechanism of diamond core bits, evaluating drilling efficiency, and optimizing tooth arrangement structures.

KEYWORDS

Diamond; Core Bit; Drilling; Cutting Mechanics; Calculation Model.

1. INTRODUCTION

The performance of drill bits directly affects drilling efficiency[1-5]. With the continuous improvement of domestic oil and gas development technology[6-10], factors such as high temperatures and pressures at the bottom of deep and ultra-deep wells, as well as increased rock hardness, drillability, and abrasiveness encountered during drilling, have a significant impact on drilling efficiency[11-12].

In 2011, Fang Jun et al. [13] conducted a comparative analysis of the failure of double-water-port ultra-high-matrix diamond core bits and ordinary diamond bits. The primary cause of failure was temperature difference stress and stress concentration between the double water ports due to inadequate cooling. In 2019, Loginov et al. [14] proposed a binder that could improve the wear resistance of diamond particles by mixing Fe-Ni-Mo additives into the diamond bit matrix. The wear resistance of the drill tool using nano-modified Fe-Ni-Mo binder was doubled compared to the initial binder. In 2021, Gao Yubin et al. [15] introduced a composite structural design for the main and auxiliary working layers of the bit, which changed the wear mechanism between the bit and rock, significantly improving drilling efficiency and average lifespan. In 2021, Wang Yanli et al. [16] developed a continuous coring bit for deep-sea hard rock, which uses a core breaker to cut the rock to a fixed length and continuously rises with the circulating medium, preventing the core from being too long and blocking the return channel. In 2023, Wang Yue et al. [17] analyzed the force on a single diamond at ultra-high speeds through numerical simulation. Compared to conventional cutting speeds, the cutting force on a single diamond at ultra-high speeds is smaller; rock breaking occurs in both

plastic and brittle modes, and the cutting force fluctuation range is smaller at ultra-high speeds, requiring less energy for rock fragmentation. In 2024, Zhao et al. [18] designed a diamond core bit with a regenerative structure for claw toes. The average torque of the two-tooth and three-tooth claw-toe diamond core bits was reduced by 10.66% and 21.81%, respectively, compared to conventional bits, and the lifespan of the three-tooth diamond core bit was increased by 1.9 times.

The basic principle of diamond cutting for rock breaking is to utilize single-crystal diamond particles to cut and fragment rocks, similar to the principle of grinding metal with a grinding wheel. The rock-breaking mechanism can be mainly divided into two processes: firstly, the crushing effect on rocks, where when sufficient drilling pressure is applied, diamond particles crush the rocks, causing localized fragmentation and crack formation and gradual expansion under high pressure; secondly, the micro-cutting effect on rocks, where diamond particles, with extremely high hardness, cut into the rock surface in a micro-cutting action, causing fine scratches and fragmentation on the rock surface, gradually breaking the rock. As shown in the figure below.

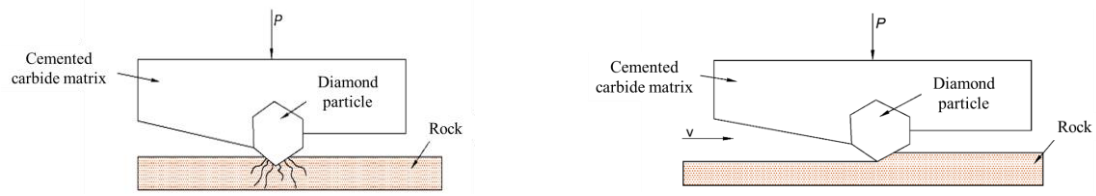

Fig. 1 Schematic Diagram of Rock-Breaking Process by Diamond Particle Cutting

This paper focuses on cutting mechanics modeling analysis for various shaped diamond cutting elements, such as rectangular, triangular, and cylindrical shapes, to explore the rock-breaking mechanism under micro-cutting conditions. Furthermore, based on the fundamental principles of elastoplastic mechanics, a cutting mechanics calculation model for axial and tangential forces of granular spherical diamonds is established.

2. MODELING OF CUTTING LOADS FOR DIAMOND PARTICLES OF DIFFERENT SHAPES

Under the same rock strength conditions, the different shapes of diamond particles result in varying force-bearing cross-sections, leading to significant differences in rock fragmentation effects and force conditions. Therefore, studying the force states of diamond particles of the same shape can clarify their respective advantages and disadvantages during use.

2.1. Rectangular Cuboid Diamond Particles

As shown in the figure below. Assuming the load coefficient for the cuboid diamond particle is q, the cutting load formula is derived as follows.

$$\frac{q'}{q} = \frac{h-y}{h} \tag{1}$$

$$q' = q - \frac{y}{h}q \tag{2}$$

$$P = \int_0^b dx \int_0^h q - \frac{y}{h}q dy = \frac{1}{2}bhq' \tag{3}$$

Where:q'— —current calculation point load coefficient, N/mm^2; h——diamond particle length, mm; b——diamond particle width, mm; x, y——Coordinate of the calculation point; F——diamond particle cutting load; N.

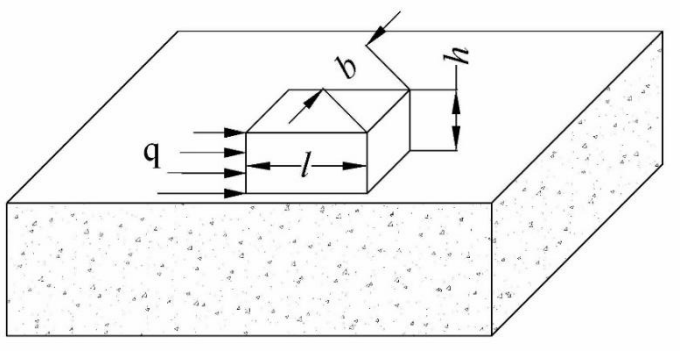

Fig. 2 Schematic Diagram of Contact between Rectangular Cross-Section and Rock

Taking a rectangular cuboid with a cross-section of as an example: $b = 1mm;\ h = 1mm$, assuming a load at a depth of 1 mm is $q' = 1\ N/mm^2$, we can obtain:$F = 0.5N$.

2.2. Triangular Prism Diamond Particles

As shown in the figure below, the cutting load formula for triangular prism diamond particles is derived as follows.

$$\frac{q'}{q} = \frac{x\tan\alpha - y}{x\tan\alpha} \tag{4}$$

$$q' = q - \frac{y}{x\tan\alpha}q \tag{5}$$

$$F = \int_0^b dx \int_0^{c\sin\alpha} q - \frac{y}{x\tan\alpha}qdy = \frac{1}{4}q'bc\sin\alpha \tag{6}$$

Where: α——top angle of the triangular cross-section°; c— —side length of the triangular cross-section, mm.

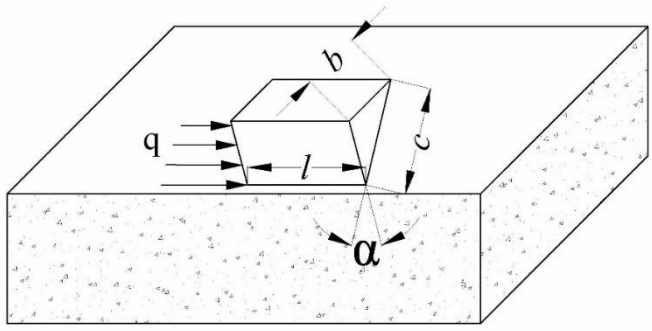

Fig. 3 Schematic Diagram of Contact between Triangular Cross-Section and Rock

Taking a triangular prism with a cross-section of as an example: $b = 1mm,\ c = \frac{\sqrt{2}}{2}mm, \alpha = \frac{\pi}{4}$, assuming a load at a depth of 1 mm is $q' = 1\ N/mm^2$, we can obtain:$F = 0.13N$.

2.3. Cylindrical Diamond Particles with Semicircular Fan-Shaped Cross-Section

As shown in the figure below, the cutting load formula for cylindrical diamond particles with semicircular fan-shaped cross-sections is derived as follows.

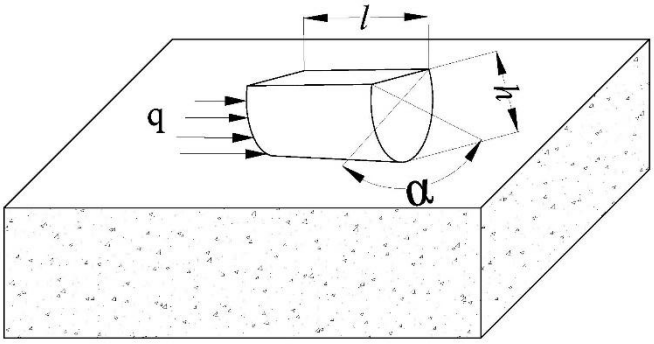

Fig. 4 Schematic Diagram of Contact between Semicircular Fan-Shaped Cross-Section and Rock

$$\frac{q'}{q} = \frac{R\cos\theta}{R} \tag{7}$$

$$q' = q\cos\theta \tag{8}$$

$$ds = R \cdot Rd\theta \tag{9}$$

$$F = \int_0^{\pi-\frac{\alpha}{2}} q\cos\theta \cdot 2R^2 d\theta = 2q'R^2 \sin\left(\pi - \frac{\alpha}{2}\right) \tag{10}$$

Where:R— —radius of the diamond particle, mm; α——semicircular fan angle°; θ——Included angle of differential area on the bottom surface.

Taking a cylinder with a cross-section of as an example: $R = 1mm,\ \alpha = \frac{2\pi}{3}$, assuming a load at a depth of 1 mm is $q' = \frac{3}{2}N/mm^2$, we can obtain: $F = 2.6N$.

2.4. Cylindrical Diamond Particles with Circular Cross-Section

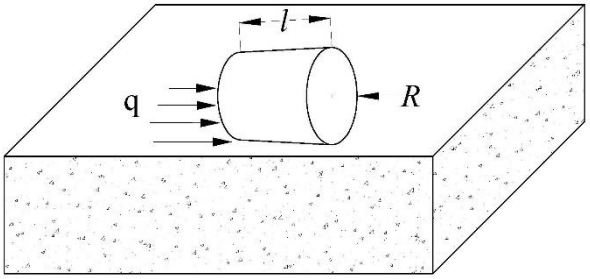

Fig. 5 Schematic Diagram of Contact between Circular Cross-Section and Rock

$$\frac{q'}{q} = \frac{R\cos\theta + R}{2R} \tag{11}$$

$$q' = \frac{1+\cos\theta}{2}q \tag{12}$$

$$ds = R \cdot Rd\theta \tag{13}$$

$$F = \int_0^{2\pi} \frac{1+\cos\theta}{2} q \cdot R^2 d\theta = q'R^2(\pi + 1) \tag{14}$$

Taking a cylinder with a cross-section of as an example: $R = 1mm$, assuming a load at a depth of 1 mm is $q' = 2\,N/mm^2$, we can obtain: $F = 4.1N$.

2.5. Hemispherical Diamond Particles

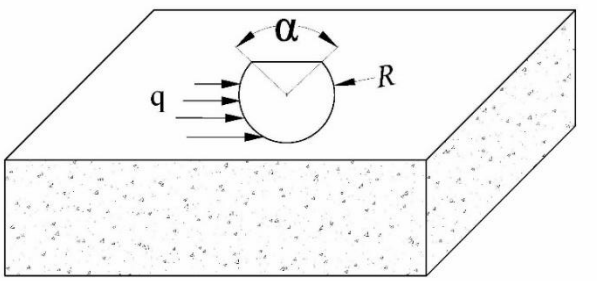

Fig. 6 Schematic Diagram of Contact between Hemispherical Cross-Section and Rock

$$\frac{q'}{q} = \frac{R\cos\theta}{R} \tag{15}$$

$$q' = q\cos\theta \tag{16}$$

$$ds = \pi R\sin\theta\, Rd\theta = \pi R^2\cos\theta \tag{17}$$

$$F = \int_0^{\pi-\frac{\alpha}{2}} q\cos\theta \cdot 2\pi R\sin\theta\, Rd\theta = \frac{1}{2}q'\pi R^2 \cdot \cos(2\pi-\alpha) \tag{18}$$

Taking a hemisphere with a cross-section of as an example: $R = 1mm,\ \alpha = \frac{2\pi}{3}$, assuming a load at a depth of 1 mm is $\mathrm{q}' = \frac{3}{2}N/mm^2$, we can obtain: $F = 0.65N$.

2.6. Spherical Diamond Particles

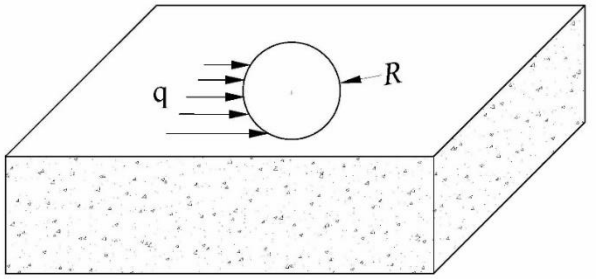

Fig. 7 Schematic Diagram of Contact between Spherical Cross-Section and Rock

$$\frac{q'}{q} = \frac{R\cos\theta + R}{2R} \tag{19}$$

$$q' = \frac{1+\cos\theta}{2}q \tag{20}$$

$$ds = \pi R\sin\theta\, Rd\theta = \pi R^2\cos\theta \tag{21}$$

$$F = \int_0^{2\pi} \frac{1+\cos\theta}{2}q \cdot \pi R\sin\theta\, Rd\theta = \frac{3}{2}q'\pi R^2 \tag{22}$$

Taking a sphere with a cross-section of as an example: $R = 1mm$, assuming a load at a depth of 1 mm is $\mathrm{q}' = 2\,N/mm^2$, we can obtain: $F = 9.4\,N$.

3. SINGLE-TOOTH PARTICLE MODEL BASED ON ELASTOPLASTIC MECHANICS

Based on the study of the diamond rock-breaking process, when a single diamond particle contacts and cuts rock, a certain degree of plastic deformation occurs[19,20]. For ease of analysis, the model is simplified to the form of a sphere in contact with a plane. During the contact process, the contact state of the two bodies transitions from elastic to plastic contact. In this contact area, both states coexist, and the contact stress should not be represented solely by the Hertz contact stress distribution formula. At this time, the contact stress is assumed to be zoned, with plastic deformation occurring in the middle part of the contact area. The contact stress in this region is uniformly distributed and equivalent to the contact stress during complete plastic deformation. The rest of the contact area undergoes elastic deformation, and the contact stress in this part exhibits a Hertz contact stress distribution, gradually decreasing from the maximum contact stress to zero. A "finite contact stress" contact stress distribution mode is proposed, as shown in the figure below.

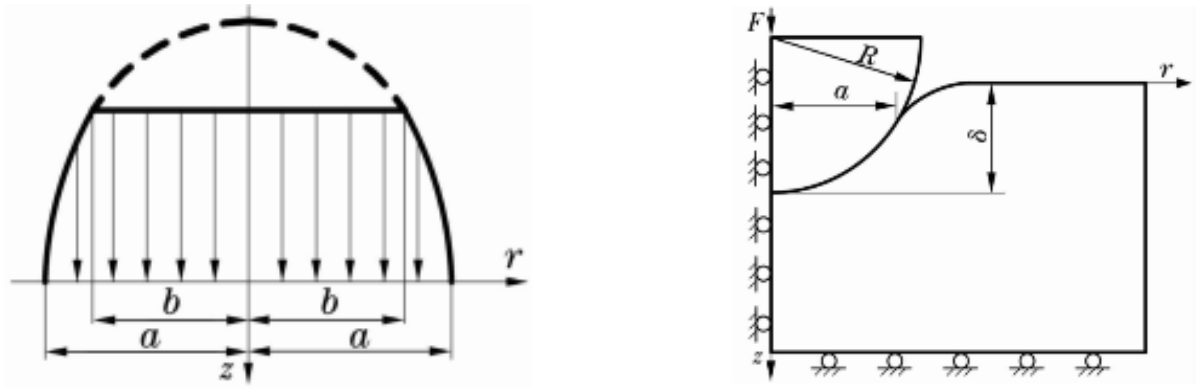

Fig. 8 Schematic Diagram of Contact Stress Distribution along the Contact Surface and Indentation Model

$$E^* = E_1/(1-{v_1}^2) + E_2/(1-{v_2}^2) \tag{23}$$

$$p(r) = \begin{cases} \dfrac{2E^*}{\pi R}\sqrt{(a^2-r^2)} & b \le r \le a \\ CR_e & 0 \le r \le b \end{cases} \tag{24}$$

$$C = 2.845 - 0.4921\frac{a}{r} \tag{25}$$

Because the contact radius a<< R, C ≈ 2.8 in Equation (4-3). However, when initial yielding occurs, p_0=1.6R_e; during complete plastic deformation, p_0= (2.8~3)R_e; therefore, C is not a constant and varies with contact depth or contact radius. Appropriate corrections are made to the "finite pressure distribution" assumption to obtain Equations (26) and (27):

$$p(r) = \begin{cases} \dfrac{2E^*}{\pi R}\sqrt{(a^2-r^2)} & b \le r \le a \\ kR_e & 0 \le r \le b \end{cases} \tag{26}$$

$$\mathrm{F} = \int_{\mathrm{b}}^{\mathrm{a}} \frac{2\mathrm{E}^*}{\pi \mathrm{R}}\sqrt{(\mathrm{a}^2-\mathrm{r}^2)}\cdot 2\pi \mathrm{r}\mathrm{d}\mathrm{r} + \int_0^{\mathrm{b}} \mathrm{k}\mathrm{R}_{\mathrm{e}}\cdot 2\pi \mathrm{r}\mathrm{d}\mathrm{r} \tag{27}$$

$$\mathrm{F} = \frac{4E^*}{3R}(a^2-b^2)^{\frac{3}{2}} + \pi k R_e b^2 \tag{28}$$

Where:

E_1, E_2——elastic moduli of the sphere and plane materials;

$v_{1,}v_2$——Poisson's ratios of the sphere and plane;

Re——yield strength of the material;

R——radius of the sphere;

a——contact radius;

b——radial distance from the center of the contact area to the boundary point between elastic and plastic contact stresses;

According to the stress continuity condition at the boundary point:

$$p(b) = kR_e = \frac{2E^*}{\pi R}\sqrt{(a^2 - b^2)} \tag{29}$$

$$b = \sqrt{a^2 - \left(\frac{\pi k R_e R}{2E^*}\right)^2} \tag{30}$$

$$F = \pi k R_e \left[a^2 - \frac{1}{3}\left(\frac{\pi k R_e R}{2E^*}\right)^2\right] \tag{31}$$

Average contact stress between the sphere and plane:

$$p_m = \frac{F}{\pi a^2} = kR_e\left[1 - \frac{1}{3}\left(\frac{\pi k R_e R}{2E^* a}\right)^2\right] \tag{32}$$

At initial yielding, the critical average contact pressure:

$$p_{my} = \frac{F_y}{\pi {a_y}^2} = 1.0752R_e \tag{33}$$

According to Hertz theory, the relationship between the contact radius and contact deformation for elastic contact between a sphere and a plane is:

$$\frac{a}{a_y} = \sqrt{\frac{2\delta}{\delta_y}} \tag{34}$$

Where $F_y,\ a_y, \sigma_y$ are the contact load, contact radius, and contact deformation when the contact deformation is at the critical yield state. Therefore, at critical yield, $\mathrm{k} = 1.466$; the value range of is 1.466~3.

Thus, we obtain:

The normal force when the diamond element indents into the rock can be obtained by integrating the load (Equation 35) and then simplified (Equation 36):

$$Fp = \int_b^a \frac{2E^*}{\pi R}\sqrt{(a^2 - r^2)} \cdot 2\pi r dr + \int_0^b kR_e \cdot 2\pi r dr \tag{35}$$

$$Fp = \frac{4E^*}{3R}(a^2 - b^2)^{\frac{3}{2}} + \pi k R_e b^2 \tag{36}$$

Similarly, the lateral force on the diamond element can be obtained by integrating (Equation 37) and then simplified (Equation 38):

$$Ft = \frac{1}{2}\left(\int_b^a \frac{2E^*}{\pi R}\sqrt{(a^2 - r^2)} \cdot 2\pi r dr + \int_0^b kR_e \cdot 2\pi r dr\right) \tag{37}$$

$$Ft = \frac{2E^*}{3R}(a^2 - b^2)^{\frac{3}{2}} + \frac{1}{2}\pi k R_e b^2 \tag{38}$$

4. SUMMARY

Diamond core bit drilling offers advantages such as good working stability, relatively high rock-breaking efficiency, and long service life. Based on the analysis of the geometric dimensions and load characteristics of diamond particles of various shapes, such as rectangular, triangular, and circular, this paper establishes a cutting load calculation model for diamond particles based on the principles of elastoplastic mechanics. This model fully considers the elastoplastic deformation of rock materials and proposes a "finite contact stress" contact stress distribution mode, which can be used to analyze the axial load, radial load, torque, etc., of the bit. The cutting mechanics analysis and calculation model for diamond particles in core bits established in this paper provides theoretical support for mastering the mechanical analysis and calculation methods of the entire bit. It has important reference value for studying the rock-breaking mechanism of bits, optimizing tooth arrangement parameters, and optimizing drilling parameters.

REFERENCES

[1] Chen Changchang, Ji Guodong, Wang Haige, et al. Safe Speed-Up Drilling Technology for Ultra Deep Well Based on Geology-Engineering Integration[J]. Springer Series in Geomechanics and Geoengineering, 2023: 2784-2798.

[2] Dvoynikov, Mikhail V; Sidorkin, Dmitrii I, Yurtaev, Sergei L, et al. Drilling of deep and ultra-deep wells for prospecting and exploration of new raw mineral fields[J]. Journal of Mining Institute, 2022, Vol. 258: 945-955.

[3] Zhu, Xiaohua; Li, Rui; Liu, Weiji, et al. Development Status of High-efficiency Rock-breaking and Speed-increasing Technologies for Deep Shale Gas Horizontal Wells[J]. Xinan Shiyou Daxue Xuebao / Journal of Southwest Petroleum University, 2023, Vol. 45(4): 1-18.

[4] Hou Zixu; Jia Xiaobin; Li Shuanggui, et al. Research on the torsion impact generator for speeding up drilling in deep formation of Yubei area[J]. Oil Drilling & Production Technology / Shiyou Zuancai Gongyi, 2013, Vol. 35(5): 132-136.

[5] Zhang Guangya, Ma Feng, Liang Yingbo, et al. Progress in global deep oil and gas exploration fields and theoretical technologies[J]. Acta Petrolei Sinica, 2015, 36(09): 1156-1166.

[6] Chen Xianwei. Current status and development trends of deep and ultra-deep well drilling technologies[J]. Chemical Engineering & Equipment, 2023, 312(01): 211-213.

[7] He Xiao, Chen Gengsheng, Wu Jianfa, et al. New progress and challenges in the exploration and development of deep shale gas in the southern Sichuan Basin[J]. Natural Gas Industry, 2022, 42(08): 24-34.

[8] Wang Haige, Huang Hongchun, Ji Guodong, et al. Progress and challenges of drilling and completion technologies for deep, ultra-deep, and horizontal wells in China[J]. China Petroleum Exploration, 2023, 28(03): 1-11.

[9] Wang Daxun, Liu Hong, Han Song, et al. Research on deep rock mechanics and deep well drilling technology[J]. Drilling & Production Technology, 2006, (03): 6-10+121.

[10] Wang Haige, Huang Hongchun, Bi Wenxin, et al. Deep and ultra-deep oil and gas well drilling technologies: Progress and prospect[J]. Natural Gas Industry B, 2022, Vol. 9(2): 141-157.

[11] Ruan Hailong, Shen Lina, Li Chun, et al. Development and application of a new PDC bit with sharp teeth for elastic-plastic tight mudstone[J]. Exploration Engineering (Rock & Soil Drilling and Tunneling), 2014, 41(12): 80-83.

[12] Wang Jialiang, Zhang Shaohe. Experimental study and rock fragmentation mechanism analysis of diamond bits with weakened matrix abrasion resistance[J]. Journal of Central South University (Natural Science Edition), 2015, 46(04): 1436-1441.

[13] Fang Jun, Yan Taining, Li Tianjun. Wear process analysis of double-nozzle ultra-high matrix diamond bit at the bottom of the hole[J]. Coal Geology & Exploration, 2011, 39(01): 74-77.

[14] Loginov P. A, Sidorenko, D. A, Bychkova M. Ya, et al. Performance of diamond drill bits with hybrid nanoreinforced Fe-Ni-Mo binder[J]. International Journal of Advanced Manufacturing Technology, 2019, Vol. 102(5-8): 2041-2047.

[15] Gao Yubin, Chen Yang. Experimental study on diamond bits for drilling hard and compact rock formations[J]. Superhard Material Engineering, 2021, 33(03): 1-6.

[16] Wang Yanli, Yin Xiantao, Yin Guole, et al. Development of a continuous core bit for deep-sea hard rock[J]. Drilling Engineering, 2021, 48(7): 26-32.

[17] Wang Yue, Zhang Kai, Li Qizhou, et al. Study on the interaction response between a single diamond particle and rock at ultra-high speeds[J]. Drilling Engineering, 2023, 50(03): 21-29.

[18] Yan Zhao, Yumin Wen, Ke Gao, et al. Study on rock-breaking mechanism and bit adaptive characteristics under the action of claw-toe impregnated diamond bit[J]. Geoenergy Science and Engineering, 2024, Vol. 2

[19] Yu W, Blanchard J P. An elastic-plastic indentation model and its solutions[J]. Journal of materials research, 1996, 11(9): 2358-2367.

[20] Jin Hongping. Testing Principle, Method, and Experimental Study of Indentation Hardness and Residual Stress Based on the Energy Method [D]. Huazhong University of Science and Technology, 2012.